Measurement of 1323 and 1487 keV resonances in $^{15}N(\alpha,\gamma)^{19}F$ with the recoil separator ERNA

A. Di Leva,[1,2,*] G. Imbriani,[1,2] R. Buompane,[2,3] L. Gialanella,[2,3] A. Best,[1,2] S. Cristallo,[4,5] M. De Cesare,[2,3,6] A. D'Onofrio,[2,3] J. G. Duarte,[2,3] L. R. Gasques,[2,3,7] L. Morales-Gallegos,[2,8] A. Pezzella,[2,9] G. Porzio,[2,3] D. Rapagnani,[5,10] V. Roca,[1,2] M. Romoli,[2] D. Schürmann,[1,2] O. Straniero,[2,4] and F. Terrasi[2,3]

(ERNA Collaboration)

[1]*Dipartimento di Fisica "E. Pancini", Università di Napoli "Federico II", Napoli, Italy*

[2]*INFN, Sezione di Napoli, Napoli, Italy*

[3]*Dipartimento di Matematica e Fisica, Università degli Studi della Campania "L. Vanvitelli", Caserta, Italy*

[4]*INAF, Osservatorio Astronomico di Collurania, Teramo, Italy*

[5]*INFN, Sezione di Perugia, Perugia, Italy*

[6]*Dipartimento di Metodologie e Tecnologie per le Osservazioni e Misure, Centro Italiano Ricerche Aerospaziali, Capua, Italy*

[7]*Departamento de Física Nuclear, Instituto de Física da Universidade de São Paulo, São Paulo, Brazil*

[8]*SUPA, School of Physics and Astronomy, University of Edinburgh, Edinburgh, United Kingdom*

[9]*Dipartimento di Scienze Chimiche, Università di Napoli "Federico II", Napoli, Italy*

[10]*Dipartimento di Fisica e Geologia, Università degli Studi di Perugia, Perugia, Italy*

(Received 31 October 2016; published 13 April 2017)

Background: The origin of fluorine is a widely debated issue. Nevertheless, the $^{15}N(\alpha,\gamma)^{19}F$ reaction is a common feature among the various production channels so far proposed. Its reaction rate at relevant temperatures is determined by a number of narrow resonances together with the direct capture and the tails of the two broad resonances at $E_{c.m.} = 1323$ and 1487 keV.

Purpose: The broad resonances widths, Γ_γ and Γ_α, have to be measured with adequate precision in order to better determine their contribution to the $^{15}N(\alpha,\gamma)^{19}F$ stellar reaction rate.

Methods: Measurement through the direct detection of the ^{19}F recoil ions with the European Recoil separator for Nuclear Astrophysics (ERNA) were performed. The reaction was initiated by a ^{15}N beam impinging onto a ^4He windowless gas target. The observed yield of the resonances at $E_{c.m.} = 1323$ and 1487 keV is used to determine their widths in the α and γ channels.

Results: We show that a direct measurement of the cross section of the $^{15}N(\alpha,\gamma)^{19}F$ reaction can be successfully obtained with the recoil separator ERNA, and the widths Γ_γ and Γ_α of the two broad resonances have been determined. While a fair agreement is found with earlier determination of the widths of the 1487 keV resonance, a significant difference is found for the 1323 keV resonance Γ_α.

Conclusions: The revision of the widths of the two more relevant broad resonances in the $^{15}N(\alpha,\gamma)^{19}F$ reaction presented in this work is the first step toward a more firm determination of the reaction rate. At present, the residual uncertainty at the temperatures of the ^{19}F stellar nucleosynthesis is dominated by the uncertainties affecting the direct capture component and the 364 keV narrow resonance, both so far investigated only through indirect experiments.

DOI: 10.1103/PhysRevC.95.045803

I. INTRODUCTION

The origin of ^{19}F is a widely debated issue in astrophysics. Several stellar environments have been proposed as F production sites: core-collapse supernovae [1], Wolf-Rayet stars [2], and asymptotic giant branch (AGB) stars [3]. Among them, only in AGB stars is fluorine synthesis confirmed by direct spectroscopic observation of [F/Fe] enhancements (see Refs. [4,5, and references therein]), and recent studies seem to exclude the first two scenarios [6,7]. It was early recognised that the $^{15}N(\alpha,\gamma)^{19}F$ reaction is a leading process for the ^{19}F production when He burning is active. Although the H burning ashes are heavily depleted in ^{15}N, which is efficiently destroyed by proton capture, these ashes are enriched in ^{14}N. Various reaction chains may lead to the production of ^{15}N nuclei at relatively low temperatures, $\sim$100 MK. A likely reaction chain is $^{14}N(n,p)^{14}C(\alpha,\gamma)^{18}O(p,\alpha)^{15}N$, which however requires an efficient neutron source. Some ^{15}N may be also produced by $^{14}N(\alpha,\gamma)^{18}F(\beta^+)^{18}O(p,\alpha)^{15}N$, where the protons need to be simultaneously released by the $^{14}N(n,p)^{14}C$ reaction. Therefore the presence of a neutron source is a key requirement. This condition is actually fulfilled in low-mass AGB stars undergoing thermal pulses, where the $^{13}C(\alpha,n)^{16}O$ reaction is known to be the main neutron source powering the *s*-process nucleosynthesis in their He-rich mantles [8]. The competition with some reactions that destroy ^{15}N and/or ^{19}F, such as $^{15}N(p,\alpha)^{12}C$, $^{19}F(n,\gamma)^{20}F$, $^{19}F(p,\alpha)^{16}O$, and $^{19}F(\alpha,p)^{22}Ne$, should also be carefully considered; see, e.g., Refs. [9,10] for recent experimental works, and Ref. [11] for a review.

The rate of the $^{15}N(\alpha,\gamma)^{19}F$ reaction at relevant AGB temperatures, 20 to 120 MK depending on the star's mass, is determined by a number of narrow resonances, the most

*Corresponding author: antonino.dileva@unina.it

important being the $E_{\rm c.m.} = 364$ keV one, together with the direct capture (DC) component and the tails of two broad resonances at $E_{\rm c.m.} = 1323$ and 1487 keV. The strength of the $E_{\rm c.m.} = 364$ keV resonance has been determined through an indirect measurement reported in Ref. [12]. Due to the model dependence of the result, an uncertainty of a factor of 2 is assumed for this quantity. In the same work the spectroscopic factors of most of the ^{19}F bound states were determined, and on the basis of a single-particle transition model the DC component has been estimated. On this latter quantity, according to the survey in Ref. [13], an uncertainty of 40% is generally assumed. The mentioned uncertainties influence the determination of the reaction rate at relevant AGB temperatures.

II. EXPERIMENTAL SETUP AND PROCEDURES

The measurement of the ^{15}N$(\alpha,\gamma)^{19}$F reaction yield was performed in inverse kinematics, i.e., a ^{15}N beam [14] impinging onto a ^{4}He windowless gas target, using the European Recoil separator for Nuclear Astrophysics (ERNA). ERNA was originally installed and commissioned at the Dynamitron Tandem Laboratorium of the Ruhr-Universität Bochum, Germany [15–17]. In 2009 it was moved to the Center for Isotopic Research on Cultural and Environmental heritage (CIRCE) laboratory in Caserta, Italy [18]. The separator underwent a major upgrade with the addition of the Charge State Selection dipole Magnet (CSSM) directly downstream of the target. A schematic view of the present ERNA layout is shown in Fig. 1. The ion beam emerging from the 3 MV tandem accelerator is transported through the CIRCE AMS beamline: a 90° analyzing magnet and an electrostatic analyzer provide the necessary ion beam purification from recoil-like contaminants. The magnetic field of the analyzing magnet is used to determine the beam energy, while its uncertainty is determined by the opening of the magnet's image slits. The settings used in the presented measurements result in a beam energy uncertainty of about 7 keV [19]. The beam is guided into the 40° beam line of ERNA by a switching magnet. A quadrupole triplet after the switching magnet is used to focus the beam onto the windowless gas target [20]. After the gas target, the separator consists sequentially of the following elements: a 30° dipole magnet (CSSM), a quadrupole triplet (QT), a Wien filter (WF1), a quadrupole singlet (QS), a 60° dipole magnet, a quadrupole doublet (QD), a Wien filter (WF2), and a detector for recoil identification and counting. Finally, several Faraday cups (FC), and slit systems are installed along the beam line for diagnostic purposes. A Si detector is placed at about 25° in the laboratory frame with respect to beam axis, and is collimated with a $\phi = 1$ mm diameter aperture in the second downstream pumping stage of the gas target. This is used to monitor the scattering rate of ^{15}N ions on the post-stripper Ar gas (see below) needed to determine the number of projectiles impinging on the target, N_p. The scattering on Ar ensures a smooth behavior of the elastic scattering yield. Determinations of the ratio of the impinging beam charge with respect to the scattering yield are performed several times between the cross section measurements.

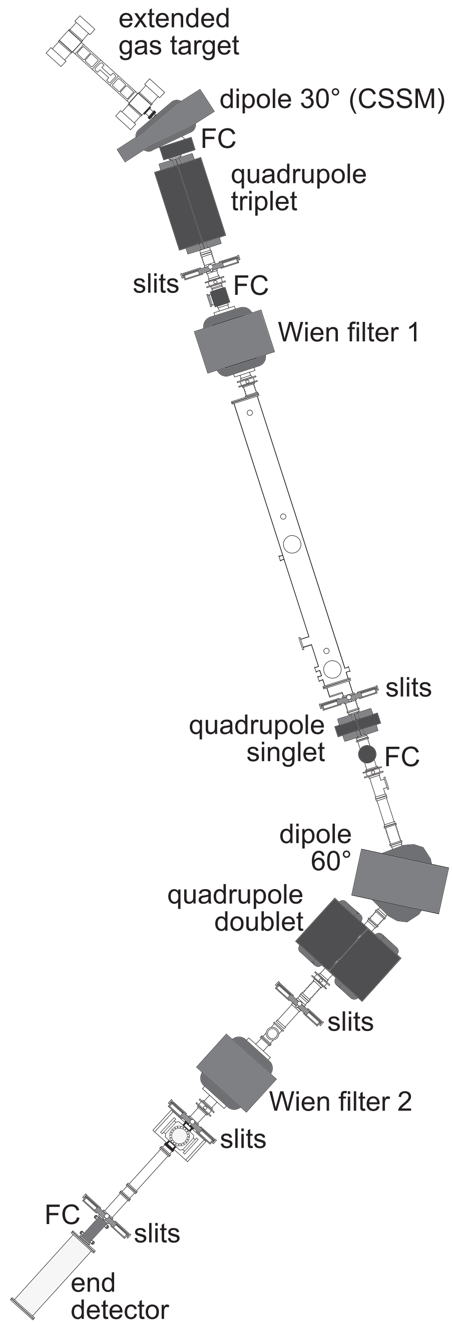

FIG. 1. Schematic view of the ERNA recoil separator.

The reaction yield is given by

$$Y_i = N_p \Phi_q T_{RMS}\, \eta \int_{E_{^{15}\rm N}-T_t}^{E_{^{15}\rm N}} \frac{\sigma(E)}{\varepsilon(E)}\, dE, \tag{1}$$

where Φ_q is the probability of recoils in the $q+$ charge state to enter the separator, T_{RMS} is the separator transmission of recoils in charge state $q+$ to the end detector, η is the detection efficiency, $E_{^{15}\rm N}$ is the beam energy, T_t is the target thickness, and $\varepsilon(E)$ is the stopping power of N ions in He. All of these quantities have to be determined in order to extract the cross section σ from the observed yield.

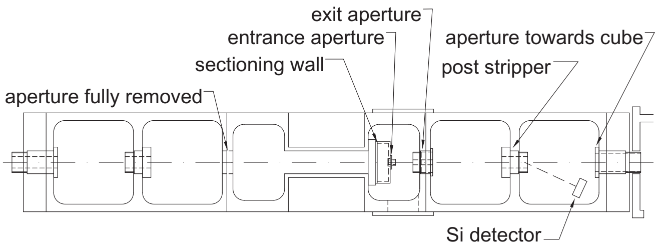

FIG. 2. Schematic top view of the modifications to the extended gas target chamber. The beam direction is from left to right. The relevant parts discussed in the text are indicated; for further details see Ref. [20].

A. ^{4}He target characterization

The recoil separator ERNA, in order to measure the ^{7}Be$(p,\gamma)^8$B, was recently provided with a windowless differentially pumped H_2 extended gas target cell [20] with an effective length of about 300 mm. This cell is too long to achieve the necessary angular acceptance for the measurement of the ^{14,15}N$(\alpha,\gamma)^{18,19}$F reaction cross sections. Therefore the central target cell was sectioned with a wall and appropriate apertures, having diameters of 6.0 mm (entrance) and 6.5 mm (exit), as schematically shown in Fig. 2. As reported in [20], in the aperture between the first and the second downstream pumping stages, Ar gas is injected in order to have an additional gas layer (post-stripper) that allows recoil ions to reach charge state equilibrium regardless of their actual reaction coordinates within the target. In order to reach the needed angular acceptance (see Sec. II C), the post-stripper aperture has a diameter of 15 mm and the aperture toward the downstream cube and the aperture between the two cube pumping stages have diameters of 24 and 27 mm, respectively.

1. Target thickness

We have determined the total target thickness through the measurement of the energy loss of several ions (see Table I), using the CSSM as an analyzer. The uncertainties are due to the ΔB determination, and to the uncertainty on the stopping power values. Operating the target at a He pressure of 4 mbar, the total thickness is $(0.54 \pm 0.03) \times 10^{18}$ atoms/cm^2.

It is worth noting that there are some issues regarding the calculation of stopping power values of N ions in He gas. This is particularly relevant since the stopping power value at resonance energy is needed to calculate the strength of a resonance from the reaction yield. In general there are not many experimental data available for gaseous targets (see, e.g., Ref. [21]); however, the stopping power of N in He was measured a significant number of times. The SRIM2003 tables appear to have a worse agreement with the experimental data than the older Ziegler 1996 calculations [21], therefore stopping power values of N in He according to this latter calculation have been used in this work. The stopping power of N in He in the energy range used in the present work is essentially determined by the data of Ref. [22], where a 2.5% systematic uncertainty is reported. However, since the Ziegler 1996 calculation is not an actual fit to the experimental data, a more conservative 5% uncertainty is assumed.

The thickness of the post-stripper alone, needed to estimate the effect on angular straggling of the recoils, was measured at a working pressure of 10 mbar, using a 2.5 MeV $^{19}F^{2+}$ beam. The observed shift in CSSM field is $\Delta B = 3.96 \pm 0.08$ mT, for a reference field of 1057.3 mT. SRIM2003 tables report for F in Ar a stopping power of 412 keV/$(1 \times 10^{18}$ atoms/cm$^2)$ at this energy, thus the corresponding thickness is $(4.5 \pm 0.5) \times 10^{16}$ atoms/cm^2. Most of the uncertainty is due to an assumed 10% error on the stopping power.

TABLE I. Measured values, results, and relevant quantities used in the target thickness determination.

Ion	E_{Lab} (MeV)	$\Delta B(^4\text{He})$ (mT)	$\varepsilon(^4\text{He})$ (keV cm^2/10^{18})	$\Delta E(^4\text{He})$ (keV)	Thickness (10^{18}/cm^2)
^{12}C	3.5	6.13	64.3	43.3 ± 3.1	0.67 ± 0.11
^{14}N	3.0	7.72	79.0	46.7 ± 2.5	0.59 ± 0.09
^{15}N	6.3	3.39	85.0	43.3 ± 4.8	0.51 ± 0.10
^{16}O	4.5	5.05	89.8	52.6 ± 3.5	0.59 ± 0.08
^{19}F	4.8	5.09	103	50.2 ± 2.7	0.49 ± 0.06
^{19}F	3.5	5.85	94.7	49.5 ± 3.0	0.52 ± 0.07

2. Density profile

The distribution of the He gas within the target cell was determined through the measurement of the yield of the broad resonance, $\Gamma_{\text{c.m.}} = 130$ keV, in ^{7}Li$(\alpha,\gamma\alpha')^7$Li at the energy of $E_{\text{lab}} = 3325$ keV, in a similar way as reported in Ref. [20]. In order to correct the observed γ-ray yield for the absorption by the chamber walls, the experimental setup was simulated with GEANT4 [23]. The simulation was validated against a measurement of the relative attenuation of an uncalibrated ^{7}Be γ-ray source that could be moved along the beam axis of the target chamber. A comparison of the experimental data with the predictions of the GEANT4 simulation is shown in Fig. 3.

The tails of the profile are well determined and account for about 25% of the total target thickness. The fact that a significant portion of the target gas is located outside the central cell is not an issue with respect to the separator acceptance if the yield of narrow resonances is to be measured, since beam energy can be adjusted to have the reaction to take place mainly at the center of the target. The effect of this feature on the measurement of nonresonant cross section is discussed in Sec. II C.

B. ^{19}F charge state probability

The Ar post-stripper equilibrium thickness for ^{19}F ions was determined through a measurement of the charge state probabilities, at several energies as a function of the stripper inlet pressure P_{stripper}. In Fig. 4 the charge state probability as a function of the post-stripper inlet pressure is shown for the case of 5 MeV $^{19}F^{3+}$ ions. On the basis of this measurement the working pressure of $P_{\text{stripper}} = 10$ mbar was chosen.

The equilibrium charge state probabilities Φ_q of ^{19}F as a function of ion speed are reported in Fig. 5. Due to the limitations of the CSSM magnetic field, not all of the charge states could be measured at all energies. In these cases, the

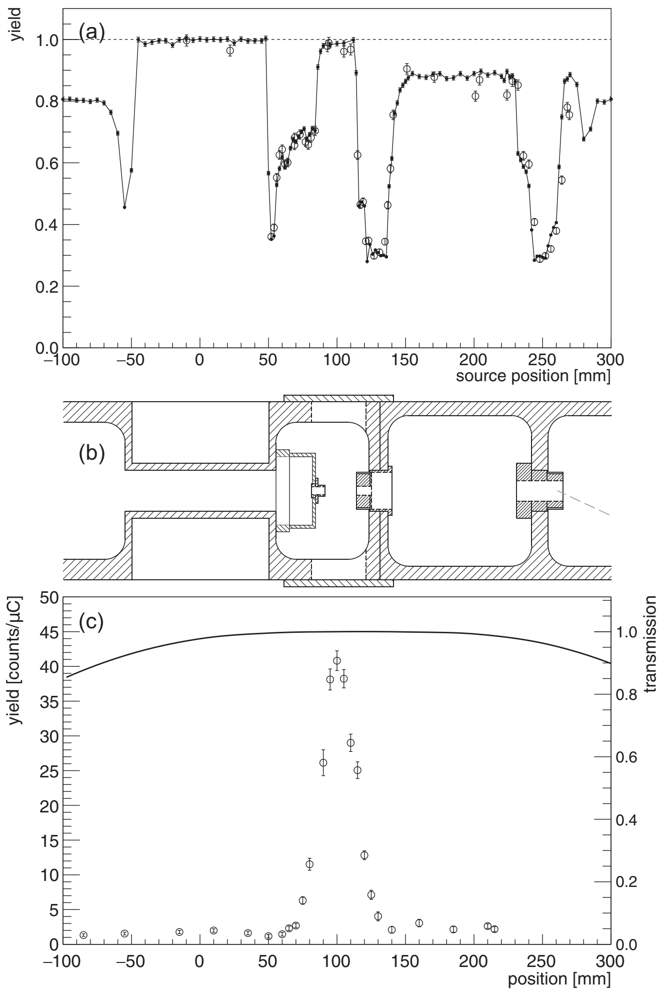

FIG. 3. (a) Target chamber's wall absorption; experimental data (open circles) are compared with the predictions of a Geant4 simulation (dots). Both measurements and simulation are scaled to unity at position ∼0 mm. (b) Detail of the target chamber top view. (c) Gas density profile of the extended ^{4}He target determined through the ^{7}Li(α,α') reaction. The experimental points (open circles) are corrected for the absorption of the target chamber, according to panel (a). The black line is the calculated transmission of recoils, in a selected charge state, to the end detector. The error bars shown in both panels (a) and (c) account for counting statistics only.

unmeasured charge state probabilities, namely of 1+ and 2+, were estimated from the measured ones. In fact at a given energy, provided that the neutral and fully stripped states are negligibly populated, the probability as a function of the charge state can be assumed to be Gaussian; see, e.g., Ref. [24]. Also the probability of a selected charge state as a function of the ion speed, in the energy range exploited, is appropriately approximated by a Gaussian as well [25], as shown in Fig. 5. There, the fits to the different charge states are not constrained by a normalization condition $\sum_q \Phi_q = 1$.

This procedure allows one to estimate the fraction of recoils that are lost because of further charge exchange in the CSSM, where some residual Ar gas is present over a relatively long distance. It turns out that $\sum_q \Phi_q \simeq 0.95$ at all energies,

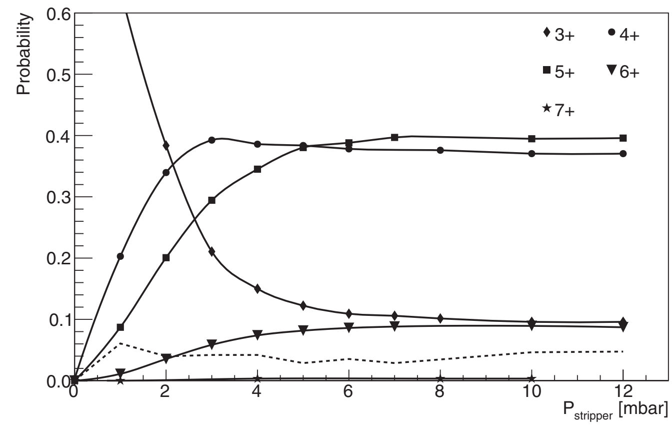

FIG. 4. Charge state probability of ^{19}F ions as a function of the Ar post-stripper inlet pressure P_{stripper} at 5.0 MeV beam energy. Lines connecting the points are to guide the eye only. The dotted line represents the unmeasured current at this energy, due to nonaccessible 1+, 2+ charge states and further charge exchanging in the CSSM chamber; see text for details.

indicating that charge exchange in the CSSM causes a loss of about 5%, independently of energy and charge state of the ions. The measured charge state probabilities should be corrected for this loss to determine their actual value at the exit of the post-stripper. However, this correction is not needed to extract the reaction cross section from the observed recoil yield, since recoils are affected by the same loss in the CSSM. The estimate of the loss of ions due to charge exchange in the CSSM has been independently confirmed by observing the variation of the beam current after the CSSM while injecting Ar gas in the CSSM chamber only.

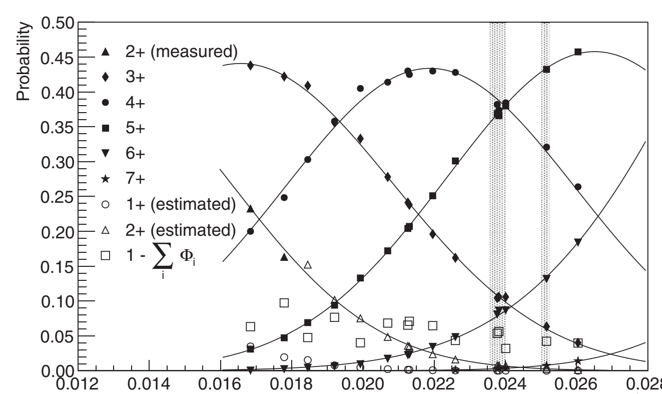

FIG. 5. Charge state probability of ^{19}F ions determined by the Ar post-stripper as a function of velocity. Filled symbols are experimentally determined values, while empty symbols are estimated values for the unmeasured 1+, 2+ charge states and for the further charge exchanging in the CSSM chamber; see text for details. Curves through points are uncorrelated Gaussian fits. Vertical shaded areas indicate the energy intervals where cross section measurements were performed.

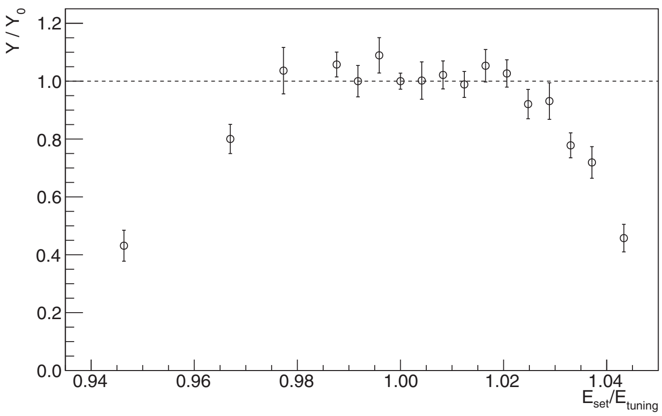

FIG. 6. Ratio of the observed yield Y with respect to the central yield Y_0 of the $E_{\mathrm{c.m.}} = 1323$ keV resonance as a function of the energy set for the separator.

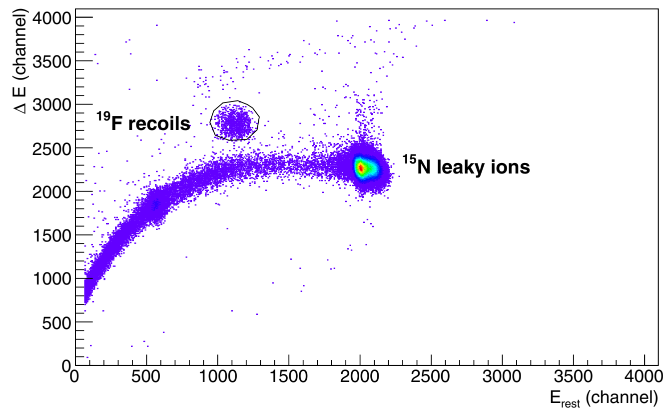

FIG. 7. Sample ICT E_{rest}-ΔE spectrum for ion identification and counting, collected at $E_{^{15}\mathrm{N}} = 7.06$ MeV.

C. Acceptance

The transmission of the recoils to the end detector, T_{RMS}, was measured to be 100% using a ^{19}F ion beam, varying the energy and angle to scan the volume of the phase space occupied by the recoils. An electrostatic deflection unit was used, in a similar way as discussed in [15,17], to mimic the recoil cone with a maximum opening angle $\vartheta_{\max}$, which is calculated according to reaction kinematics and straggling effects due to the interaction with target and post-stripper gas.

As a further test of the separator acceptance, we have used the yield of the $E_{\mathrm{c.m.}} = 1323$ keV resonance. A scan of the target was performed and then the energy of the beam was set to the middle of the plateau. Then several measurement were performed, varying the energy to which the separator was *tuned*. Results are shown in Fig. 6. The experimental points show a flat-top plateau, indicating a broad region of full acceptance, and then the reaction yield sharply drops, indicating that the limit of the energy acceptance, or the limit of angular acceptance, or both, is reached.

Moreover, reaction yield measurements of the 1323 keV resonance performed in the 3+ and 4+ charge states, characterized by quite different charge state probabilities, have given very consistent results; see Fig. 8(a).

III. EXPERIMENTAL RESULTS AND ANALYSIS

The reaction yield of the two broad resonances at 1323 and 1487 keV, corresponding to the ^{19}F states at $E_x = 5337$ and 5500.7 keV respectively, was measured. Ion identification and counting was done using an ionization chamber with a fractioned anode as an E_{rest}-ΔE telescope (ICT) [26]. In Fig. 7 a sample spectrum is reported; as can be seen the ^{19}F recoil ions are clearly separated from the leaky ^{15}N ions, i.e., primary beam ions that, due mostly to elastic scattering on the gas target apertures, make their way to the end detector. The reaction yield as a function of energy is shown in Fig. 8.

Since both resonances are relatively broad, the expected yield has been calculated through the convolution of the resonance cross section $\sigma_{BW}(E)$ and the target profile according to Eq. (1). The stopping power of N ions in He has a negligible variation over the target thickness, and the average value of 77.2 keV cm^2/10^{18} atoms is used for the analysis of both resonances. The cross section $\sigma_{BW}(E)$ is calculated using the

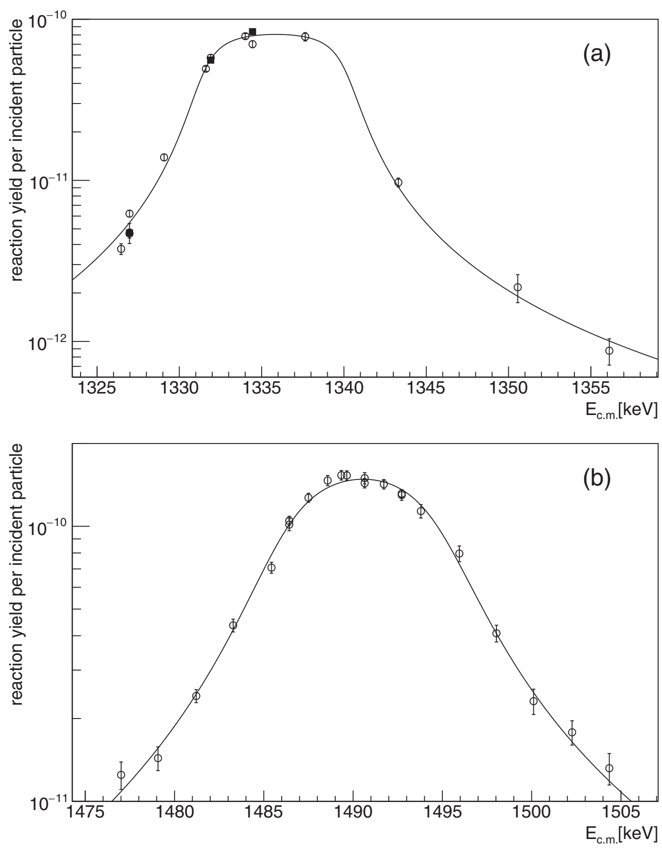

FIG. 8. Reaction yield per incident projectile observed for the two broad resonances at 1323 and 1487 keV, panels (a) and (b) respectively. Open circles and filled squares indicate measurements of recoils in the 4+ and 3+ charge states, respectively.

Breit-Wigner formula

$$\sigma_{BW}(E) = \pi \lambda^2 \frac{2J+1}{(2J_t+1)(2J_p+1)} \frac{\Gamma_\alpha(E)\Gamma_\gamma(E)}{(E_R-E)^2+\left(\frac{\Gamma(E)}{2}\right)^2}, \tag{2}$$

where λ is the projectile reduced de Broglie wavelength, J, J_t, J_p are the total angular momenta of the resonance, the target nucleus, and the projectile, respectively, E_R is the resonance energy, and Γ_α and Γ_γ are the observed partial widths. Their energy dependence is calculated according to [27]

$$\Gamma_\alpha(E) = 2P_\alpha(E)\gamma_\alpha^2, \tag{3}$$

where γ_α^2 is the observed reduced width and $P_\alpha(E)$ is the penetration factor

$$P_\alpha(E) = R\left(\frac{k}{F_l^2+G_l^2}\right),$$

with the radius $R = 5.07$ fm, calculated from the mass numbers of projectile and target, A_p and A_t, respectively, with the commonly used formula $1.25(A_p^{\frac{1}{3}} + A_t^{\frac{1}{3}})$ fm; however, the final results depend very weakly on this choice. F_l and G_l are the regular and irregular Coulomb wave functions, respectively, while

$$\Gamma_\gamma(E) = \Gamma_\gamma(E_R)\sum_i B_{\gamma i}\left[\frac{E+Q-E_{xi}}{E_R+Q-E_{xi}}\right]^{2L_i+1}, \tag{4}$$

where $Q = 4014$ keV is the reaction Q value, $B_{\gamma i}$ is the primary γ-ray branching ratio to the final state having excitation energy E_{xi}, and L_i is the multipolarity of the ith γ-ray transition. The $B_{\gamma i}$ values are taken from the ENSDF database [28]. While the multipolarity of the primary transitions are known for the 1487 keV resonance, they are not known for the 1323 keV resonance and are assumed to be 1. However, it has to be noted that the energy dependent term of Eq. (4) differs from unity at most by a fraction of a percent over the measurement energy range even in case of transitions of multipolarity 2.

Fits of $\sigma_{BW}(E)$, according to Eq. (1), to the experimental data are performed using a least-squares function (LSF). The expected yields calculated according to our best fit values are shown in Fig. 8.

In order to exclude the possibility that our results might be an artifact of a wrong target thickness determination rather than a sizeably larger resonance total width ($\simeq\Gamma_\alpha$), a study of the correlation of these two quantities has been performed. This check was done by choosing uniformly distributed random values for T_t and Γ_α that were kept fixed, and the LSF was minimized with respect to the other parameters, namely resonance energy E_R and Γ_γ. Results are shown, for both resonances, in Fig. 9. Our determination of the target thickness T_t leads to fit of the data with a LSF close to the absolute minimum, for both resonances, thus excluding possible issues with respect to this aspect. Literature values for Γ_α would lead to LSF minimum values quite far from the absolute minimum.

It has to be noted that, even at the absolute minimum, the LSF for the 1323 keV resonance shows quite high values (reduced $\chi^2 \sim 20$). Therefore for the calculation of

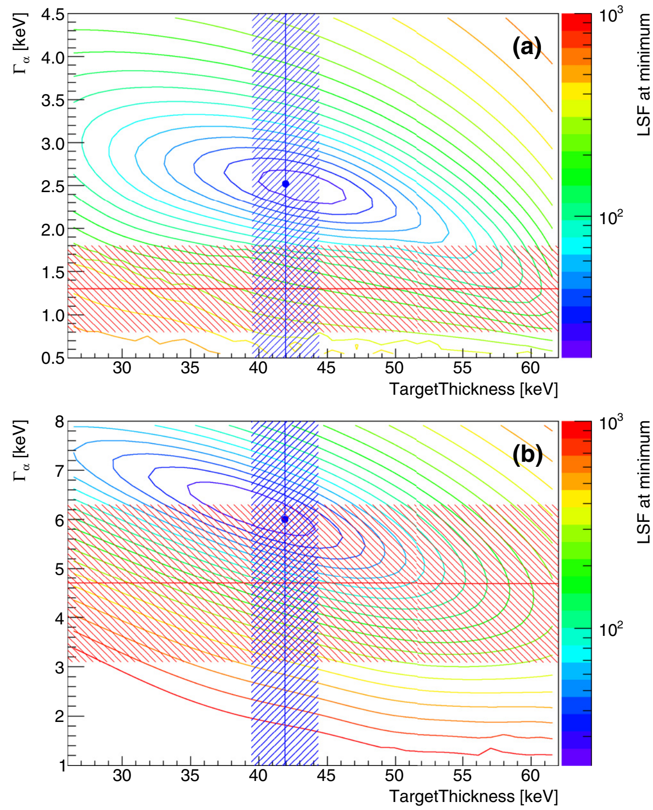

FIG. 9. LSF minima contour plots, as a function of the target thickness and Γ_α, for the 1.323 and 1.487 MeV resonances, panels (a) and (b), respectively. The vertical line is the experimentally determined target thickness and the shaded area its uncertainty. Horizontal lines are literature values of Γ_α and shaded area their uncertainties. The dots indicate the best fit values.

the LSF in the fit of the 1323 keV resonance, the statistical uncertainty of the experimental points has been inflated by a factor of 1.5. However this inflation has no influence on final parameter values nor on the final uncertainties estimation, since these are obtained through a Monte Carlo (MC) procedure, described below, rather than the error matrix at LSF minimum.

The recommended values and uncertainty on the resonances parameters, reported in Table II, are obtained through a MC

TABLE II. Parameters of the measured resonances as obtained from the MC procedure. Most of the uncertainty on the E_R values is due to the beam energy determination.

	This work	Ref. [29]	Ref. [30]
	1323 keV resonance		
E_R (keV)	1331.4 ± 1.6	1323 ± 2	
Γ_γ (eV)	1.62 ± 0.09		1.69 ± 0.14
Γ_α (keV)	2.51 ± 0.10		1.3 ± 0.5
	1487 keV resonance		
E_R (keV)	1486.1 ± 1.9	1486.7 ± 1.7	
Γ_γ (eV)	2.2 ± 0.2	2.13	1.78 ± 0.17
Γ_α (keV)	6.0 ± 0.3	4 ± 1	4.7 ± 1.6

TABLE III. Relative uncertainties affecting overall normalization: charge state probability $\delta\Phi_q$, number of incident projectiles δN_p, and stopping power $\delta\varepsilon_{^{15}\mathrm{N}}$. Uncertainty on current integration is 3% at all energies.

Resonance energy (keV)	$\delta\Phi_q$	δN_p	$\delta\varepsilon_{^{15}\mathrm{N}}$
1323	2.1%	2.2%	5.0%
1487	3.2%	4.0%	5.0%

procedure, so that besides the statistical uncertainty also the uncertainties on the target thickness and the other quantities contributing to the overall systematic uncertainty are correctly reflected in the results. In the MC procedure 5000 fits are performed. For each fit a pseudo-dataset is generated through a Gaussian distribution of the measured values, used as central values, with the uncertainty as standard deviation; in addition the target thickness and an overall normalization parameter are set to randomly generated values. The target thickness is generated according to a normal distribution, while the normalization parameter is in part normally distributed, according to charge state probability, scattering rate, and stopping power uncertainties, as reported in Table III, and in part uniformly distributed, according to current reading uncertainty, estimated to be 3% at all energies. Then the LSF is minimized with respect to parameters E_R, Γ_α, and Γ_γ. The parameters' distributions are shown in Fig. 10. Some of the distributions obtained are slightly asymmetric but still rather close to normal. Therefore best value and uncertainty are obtained through a Gaussian fit to the histograms; the uncertainty on beam energy determination, that contributes to δE_R, is added afterwards.

Our determination of E_R for the lower energy resonance is significantly different from the literature value of 1323 keV

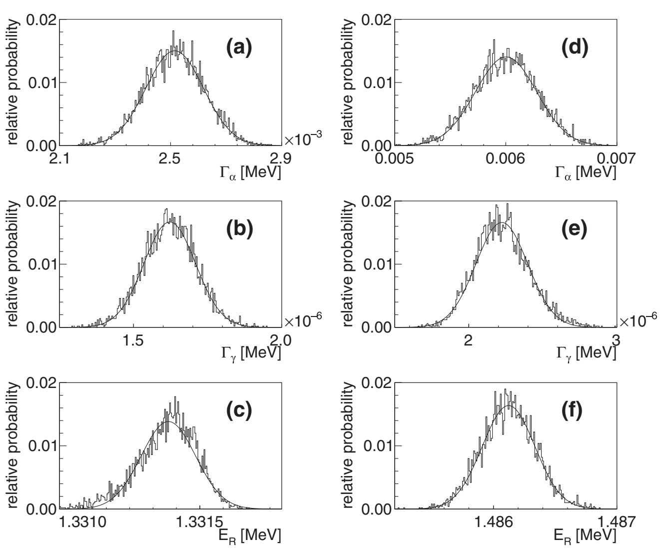

FIG. 10. Parameter value distributions, $\Gamma_\alpha,\Gamma_\gamma,E_R$ of the 1323 keV resonance, panels (a), (b), and (c) respectively, and of the 1487 keV resonance, panels (d), (e), and (f), as obtained from the MC procedure.

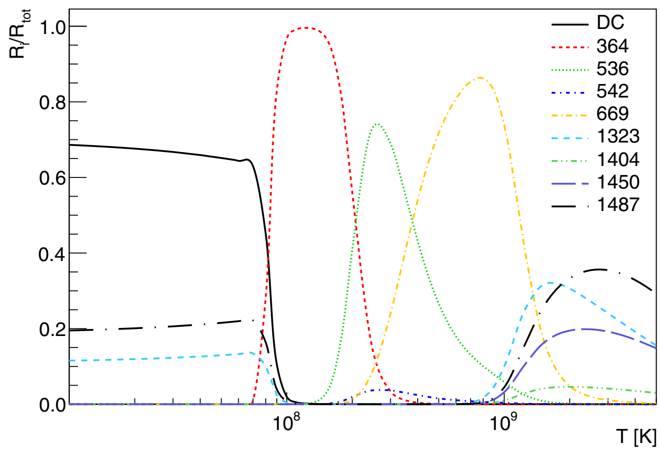

FIG. 11. Fractional contribution of resonances and DC component to the total reaction rate of the $^{15}\mathrm{N}(\alpha,\gamma)^{19}\mathrm{F}$, as a function of the temperature. The resonances are identified with their center-of-mass energy in keV.

reported in [29], that in turn is based on the data of [31], while it is in excellent agreement with the determination of [32]. It is worth noting that [29], as regards this resonance, makes also a reference to [33]. The 1323 keV resonance is not explicitly discussed in [33], however, the resonance profile shown in Fig. 23, panel g of that work, appears to be consistent with a larger E_R value. In addition our determination of E_R is in good agreement with values derived from experiments other than $^{15}\mathrm{N}(\alpha,\gamma)^{19}\mathrm{F}$ [29].

As concerns the widths, the Γ_γ and Γ_α values obtained in the present work for the 1487 keV resonance are compatible with earlier determinations ([30], and references therein); also the 1323 keV resonance Γ_γ is found to be in an excellent agreement with literature value, while a significant difference is found for the Γ_α. Most notably the precision on the Γ_α values has been improved to about 5%.

IV. CONCLUSIONS

The recoil separator ERNA has been used to directly measure the reaction yield of the two broad resonances at $E_{\mathrm{c.m.}} = 1323$ and 1487 keV. On the basis of the experimental data their Γ_γ and Γ_α are determined. While agreement within uncertainty is found with earlier determination of the 1487 keV resonance widths, a significant difference is found for the 1323 keV Γ_α. The improved determination of the broad resonances widths significantly influences the reaction rate, and its uncertainty, at temperatures lower than 100 MK, relevant for AGB nucleosynthesis. However, at low temperatures the reaction rate is dominated by the DC component and the narrow resonance at $E_{\mathrm{c.m.}} = 364$ keV. Both components are presently known only through indirect measurements [12] and, as mentioned, are affected by large uncertainties. In Fig. 11 the contribution of each resonance with respect to the total reaction rate is shown as a function of the temperature. It is worth noting that fractional contributions to the reaction rate presented in Fig. 11 are calculated according to central values and do not bring any information on the uncertainties. As mentioned the DC component and the $E_{c.m.} = 364$ keV are largely uncertain, and therefore the relative contributions may vary sizeably.

The two investigated resonances contribute to the low temperature reaction rate through their tails. Our new determination of the Γ_α's increases their contribution to the reaction rate by about 15% at relevant astrophysical energies, with respect to the rate calculated according to literature values. The related astrophysical implications will be discussed elsewhere.

We plan to extend the measurements towards lower energies, hopefully as far as to directly determine the strength of the $E_{c.m.} = 364$ keV resonance that is presently known only through indirect measurements [12] with a factor of 2 of uncertainty. Moreover, also a direct determination of the DC component at around $E_{c.m.} \sim 1$ MeV appears to be possible.

ACKNOWLEDGMENTS

The authors want to commemorate M. Romano and N. De Cesare who, since its beginning, gave an invaluable contribution to the ERNA project. Their early demise is an irreplaceable loss for our Collaboration and for the experimental nuclear physics community. The Authors thank F. de Oliveira for enlightening discussions. This work was supported by INFN and by MIUR under the grants FIRB RBFR08549F and PRIN 20128PCN59. L.R.G. acknowledges financial support under the grants FAPESP 2014/11670-0 and Internationalization Program UCLV 2016.

[1] S. E. Woosley and W. C. Haxton, Nature (London) **334**, 45 (1988).
[2] G. Meynet and M. Arnould, Astron. Astrophys. **355**, 176 (2000).
[3] M. Forestini, S. Goriely, A. Jorissen, and M. Arnould, Astron. Astrophys. **261**, 157 (1992).
[4] A. Jorissen, V. V. Smith, and D. L. Lambert, Astron. Astrophys. **261**, 164 (1992).
[5] C. Abia, A. Recio-Blanco, P. de Laverny, S. Cristallo, I. Domínguez, and O. Straniero, Astrophys. J. **694**, 971 (2009).
[6] S. R. Federman, Y. Sheffer, D. L. Lambert, and V. V. Smith, Astrophys. J. **619**, 884 (2005).
[7] A. Palacios, M. Arnould, and G. Meynet, Astron. Astrophys. **443**, 243 (2005).
[8] O. Straniero, R. Gallino, M. Busso, A. Chiefei, C. M. Raiteri, M. Limongi, and M. Salaris, Astrophys. J. Lett. **440**, L85 (1995).
[9] G. Imbriani, R. J. deBoer, A. Best, M. Couder, G. Gervino, J. Görres, P. J. LeBlanc, H. Leiste, A. Lemut, E. Stech, F. Strieder, E. Uberseder, and M. Wiescher, Phys. Rev. C **85**, 065810 (2012).
[10] I. Lombardo, D. Dell'Aquila, A. Di Leva, I. Indelicato, M. La Cognata, M. La Commara, A. Ordine, V. Rigato, M. Romoli, E. Rosato, G. Spadaccini, C. Spitaleri, A. Tumino, and M. Vigilante, Phys. Lett. B **748**, 178 (2015).
[11] S. Cristallo, A. Di Leva, G. Imbriani, L. Piersanti, C. Abia, L. Gialanella, and O. Straniero, Astron. Astrophys. **570**, A46 (2014).
[12] F. de Oliveira, A. Coc, P. Aguer, C. Angulo, G. Bogaert, J. Kiener, A. Lefebvre, V. Tatischeff, J.-P. Thibaud, S. Fortier, J. Maison, L. Rosier, G. Rotbard, J. Vernotte, M. Arnould, A. Jorissen, and N. Mowlavi, Nucl. Phys. A **597**, 231 (1996).
[13] R. Longland, C. Iliadis, A. E. Champagne, J. R. Newton, C. Ugalde, A. Coc, and R. Fitzgerald, Nucl. Phys. A **841**, 1 (2010).
[14] A. Di Leva, A. Pezzella, N. De Cesare, A. D'Onofrio, L. Gialanella, M. Romano, M. Romoli, D. Schuermann, F. Terrasi, and G. Imbriani, Nucl. Instrum. Methods A **689**, 98 (2012).
[15] D. Rogalla, D. Schürmann, F. Strieder, M. Aliotta, N. De Cesare, A. Di Leva, C. Lubritto, A. D'Onofrio, L. Gialanella, G. Imbriani, J. Kluge, A. Ordine, V. Roca, H. Röcken, C. Rolfs, M. Romano, F. Schümann, F. Terrasi, and H. P. Trautvetter, Nucl. Instrum. Methods A **513**, 573 (2003).
[16] L. Gialanella, D. Schürmann, F. Strieder, A. Di Leva, N. De Cesare, A. D'Onofrio, G. Imbriani, J. Klug, C. Lubritto, A. Ordine, V. Roca, H. Röcken, C. Rolfs, D. Rogalla, M. Romano, F. Schümann, F. Terrasi, and H. P. Trautvetter, Nucl. Instrum. Methods A **522**, 432 (2004).
[17] D. Schürmann, F. Strieder, A. Di Leva, L. Gialanella, N. De Cesare, A. D'Onofrio, G. Imbriani, J. Klug, C. Lubritto, A. Ordine, V. Roca, H. Rocken, C. Rolfs, D. Rogalla, M. Romano, F. Schumann, F. Terrasi, and H. P. Trautvetter, Nucl. Instrum. Methods A **531**, 428 (2004).
[18] F. Terrasi, D. Rogalla, N. De Cesare, A. D'Onofrio, C. Lubritto, F. Marzaioli, I. Passariello, M. Rubino, C. Sabbarese, G. Casa, A. Palmieri, L. Gialanella, G. Imbriani, V. Roca, M. Romano, M. Sundquist, and R. Loger, Nucl. Instrum. Methods B **259**, 14 (2007).
[19] R. Buompane *et al.* (unpublished).
[20] D. Schürmann, A. Di Leva, L. Gialanella, M. De Cesare, N. De Cesare, G. Imbriani, A. D'Onofrio, M. Romano, M. Romoli, and F. Terrasi, Eur. Phys. J. A **49**, 80 (2013).
[21] https://www-nds.iaea.org/, accessed October 2016.
[22] J. L. Price, D. G. Simons, S. H. Stern, D. J. Land, N. A. Guardala, J. G. Brennan, and M. F. Stumborg, Phys. Rev. A **47**, 2913 (1993).
[23] S. Agostinelli *et al.*, Nucl. Instrum. Methods A **506**, 250 (2003).
[24] I. S. Dmitriev and V. S. Nikolaev, ZhETF **47**, 615 (1965) [Sov. Phys. JETP **20**, 409 (1965)].
[25] R. O. Sayer, Rev. Phys. Appl. **12**, 1543 (1977).
[26] D. Rogalla, S. Theis, L. Campajola, A. D'Onofrio, L. Gialanella, U. Greife, G. Imbriani, A. Ordine, V. Roca, C. Rolfs, M. Romano, C. Sabbarese, F. Schümann, F. Strieder, F. Terrasi, and H. P. Trautvetter, Nucl. Instrum. Methods A **437**, 266 (1999).
[27] C. Iliadis, *Nuclear Physics of Stars* (Wiley-VCH Verlag, Wenheim, 2007).
[28] ENSDF, Evaluated and compiled nuclear structure data, accessed September 2016.
[29] D. R. Tilley, H. R. Weller, C. M. Cheves, and R. M. Chasteler, Nucl. Phys. A **595**, 1 (1995).
[30] S. Wilmes, V. Wilmes, G. Staudt, P. Mohr, and J. W. Hammer, Phys. Rev. C **66**, 065802 (2002).
[31] D. W. O. Rogers, R. P. Beukens, and W. T. Diamond, Can. J. Phys. **50**, 2428 (1972).
[32] P. C. Price, Proc. Phys. Soc. A **70**, 661 (1957).
[33] H. Kräwinkel, H. W. Becker, L. Buchmann, J. Görres, K. U. Kettner, W. E. Kieser, R. Santo, P. Schmalbrock, H. P. Trautvetter, A. Vlieks, C. Rolfs, J. W. Hammer, R. E. Azuma, and W. S. Rodney, Z. Phys. A **304**, 307 (1982).